GEOCHEMISTRY OF AN ABANDONED LANDFILL CONTAINING COAL COMBUSTION WASTE: IMPLICATIONS FOR REMEDIATION

Christopher Barton[1], Linda Paddock[2], Christopher Romanek[2,3], and John Seaman[2]

[1]USDA Forest Service, Center for Forested Wetlands Research, c/o Savannah River Ecology Laboratory, Drawer E, Aiken, SC 29802

[2]University of Georgia, Savannah River Ecology Laboratory, Drawer E, Aiken SC 29802

[3]Department of Geology, University of Georgia, Athens, GA 30602

1. ABSTRACT

The 488-D Ash Basin (488-DAB) is an unlined, earthen landfill containing approximately one million tons of dry ash and coal reject material at the U.S. Department of Energy's Savannah River Site, SC. The pyritic nature of the coal rejects has resulted in the formation of acidic drainage (AD), which has contributed to groundwater deterioration and threatened biota in adjacent wetlands. Establishment of a dry cover is being examined as a remedial alternative for reducing AD generation within this system by minimizing the contact of oxygen and water to the waste material. To determine the potential benefit of a cover on pore water chemistry, a series of flow-through column experiments were performed under varying environmental conditions using materials from the site. The experiment was designed to demonstrate the influence of temperature, gaseous composition (dissolved nitrogen vs. oxygen), and flow regime (continuous flow vs. episodic wetting/drying) on effluent chemistry. Results indicated that the fluid composition (e.g., pH, redox, elemental composition) was closely associated to dissolved and/or gaseous oxygen content and wetting regime. Given these conditions, the use of a dry cover could reduce the production of acid lechate over time, pending that it retards or eliminates fluid and oxygen transport to the subsurface.

Chemistry of Trace Elements in Fly Ash, edited by Sajwan *et al.*
Kluwer Academic/Plenum Publishers, 2003

2. INTRODUCTION

The degradation of water resources from coal mining and coal combustion activities is a problem of global significance. Acidic drainage (AD), a low pH water enriched in iron, aluminum, sulfate and trace elements (e.g., lead, selenium, arsenic, mercury, zinc), is formed upon exposure of pyrite to the oxidizing forces of air and water. Pyrite (FeS_2), the most common sulfide mineral on Earth, is often found within coal seams and their associated geologic strata. Once disturbed or extracted during the mining process, pyrite oxidation and AD generation may begin and can continue for thousands of years. Moreover, since pyrite is found within coal seams, AD is not solely a "mining" problem and may occur anywhere that pyrite enriched coal or its byproducts are stored. In the United States alone, approximately 20,000 km of streams and over 72,000 ha of lakes and reservoirs are impacted by AD[1].

The oxidation of sulfide minerals and formation of AD is a complex process involving hydrolysis, redox, and microbial reactions[2]. The general stoichiometry can be described by the following reactions:

$$2FeS_{2(s)} + 7O_2 + 2H_2O \rightarrow 2Fe^{2+} + 4SO_4^{2-} + 4H^+ \quad [1]$$

$$Fe^{2+} + 0.25O_2 + H^+ \rightarrow Fe^{3+} + 0.5H_2O \quad [2]$$

$$Fe^{3+} + 3H_2O \rightarrow Fe(OH)_{3(s)} + 3H^+ \quad [3]$$

$$FeS_{2(s)} + 14Fe^{3+} + 8H_2O \rightarrow 15Fe^{2+} + 2SO_4^{2-} + 16H^+ \quad [4]$$

where iron sulfide and other mixed-metal sulfides decompose upon exposure to the atmosphere, producing ferrous iron, sulfate and proton acidity [1]. The partial oxidation of ferrous to ferric iron consumes some protons [2]. However, ferric iron may act as an electron acceptor and contribute to additional acid production through hydrolysis [3] and/or further pyrite oxidation [4]. Subsequently, acids produced from the oxidation may dissolve minerals and mobilize metals from materials found in the surrounding environment (coal, ash, soil etc.).

The oxidation of ferrous to ferric iron was determined by Singer and Stumm[3] to be the rate-limiting step in the generation of AD. Further, these researchers showed that the oxidation of Fe^{2+} is pH dependent and extremely slow at pH $\approx$3.0. However, the bacteria *Thiobacillus thiooxidans*, a sulfur-oxidizing bacteria, and *Thiobacillus ferrooxidans*, a chemosynthetic iron-oxidizing bacteria, were found to act as catalysts and accelerate the oxidation of ferrous sulfide to ferric sulfate at pH levels below 4.0[4]. Singer and Stumm[3] demonstrated that the rate of Fe^{2+} oxidation in an untreated mine sample was 10^6 times greater than that observed in a sterilized sample. As such, the rate of pyrite oxidation may be influenced not only by redox conditions, but also by environmental conditions that may affect the microbial communities (i.e., temperature and pH).

Several innovative techniques have been proposed to reduce AD generation by limiting the exposure of pyrite to air and water. Inundation is a basic application of this concept. The diffusion coefficient of dissolved oxygen in water is approximately 10,000 times lower than that in the gas phase. As such, oxygen-consuming reactions are greatly reduced upon flooding of pyrite-bearing materials and bacterially enhanced pyrite oxidation is diminished. However, equation [4] (above) indicates that oxidation of pyrite may continue as long as ferric iron is present. Hence, long-term stagnation or bacterially mediated hypoxia must also occur to maintain a reducing environment and hold iron in the ferrous state.

A dry cover is an innovative technology that utilizes a layer of soil, compost or other organic material (peat, hay, straw, sawdust) above mining waste to deplete oxygen through bacterial consumption[5]. The organic waste may also inhibit oxidation by removal of Fe^{3+} from solution through complexation, and the formation of pyrite-Fe^{2+}-humate complexes[6]. Changes in the particle size distribution of the cover over that of the mining waste may also be engineered to enhance water storativity. As such, water percolation through the waste and exposure to the pyrite could be decreased. Under such a scenario, the use of vegetation may also be included to aid in the removal of water through

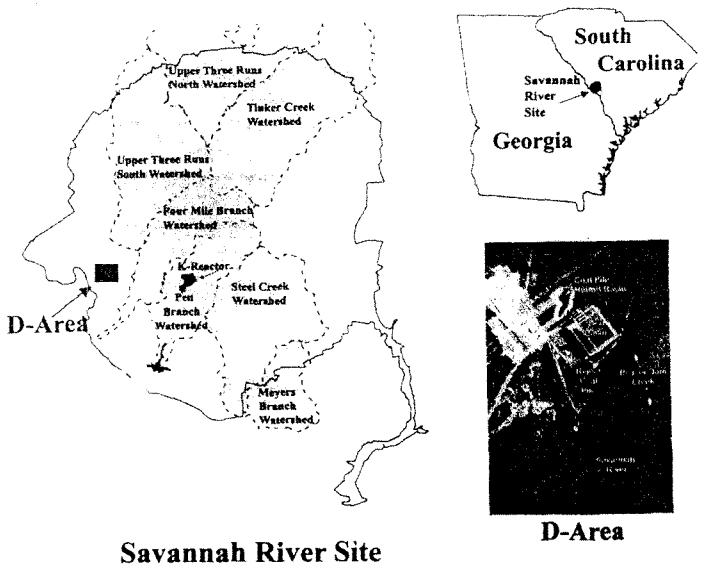

Figure 1. D-Area power plant and vicinity on the Savannah River Site, SC.

evapotranspiration[7]. On a large scale, the net effect of these techniques is to cut off the oxygen source. On a microscopic scale, these techniques may also aid in preventing oxidation by altering the surface chemistry of pyrite. Several researchers have shown that soluble organic acids from the breakdown of litter, and colloidal silicate and phosphate salts from soils may act as passivating agents through the formation of a surface coating, which may render pyrite impenetrable to oxidative attack[6,8,9].

Establishment of a dry cover is being examined as a remedial alternative for reducing AD generation within the 488-D Ash Basin (488-DAB) at the U.S. Department of Energy's Savannah River Site, SC. In order to determine the potential benefits of a cover, a series of column experiments was conducted to determine the effect of temperature and wetting regime on surficial materials collected from the 488-DAB. Data from these experiments are used to predict the chemistry of lechate anticipated under various field conditions.

3. MATERIALS AND METHODS

3.1. Site Description and Background

The 488-DAB is an unlined, earthen containment basin located on the Savannah River Site, SC that received sluiced fly ash, dry fly ash and coal reject material from the early 1950's to the mid 1990's (Figure 1). Non hazardous wastes deposited in the basin contain metals typical of fly ash and coal (As, Co, Cr, Cu, Fe, Mn, Ni and Zn). The 488-DAB is ~1,800' x 600' x 18' in size and contains ~19 x 10^6 ft^3 of waste material. The basin was constructed on the existing land surface at ~35m (msl) and is ~9m above the Savannah River. The present surface of the basin is at ~40 to 37' (msl), sloping gently to the west and it is filled with waste, except in the far western reach where surface waters collect during rainfall events.

The extent of water-saturated material in 488-DAB is not known, nor if any communication exists between basin waste and the local water table. Based on limited soil borings, the waste seems to be variably saturated, having both wet and dry zones that vary with depth. The source of this water may be meteoric infiltration or lateral groundwater flow from adjacent basins (488-1D, -2D and -4D). Hydraulic anisotropies may have been created when various materials were introduced to the basin. Alternatively, post-depositional features such as diagenetic "hard pans" may have developed as materials weathered over time, creating local anisotropies

3.2. Column Construction

A 2 x 1 x 1 m deep trench was excavated in the center of 488-DAB to retrieve material for the column study. Six horizons were noted in a cross-section of the trench; of these, a coal rubble zone (A) and fly ash residue zone (D) best represented the character of the waste and were chosen for additional study. In the field, zone A consisted of poorly-sorted, pebble-sized pieces of coal and pyrite, while zone D contained a relatively uniform fine-grained material. Approximately 1 m^3 of material was shoveled from zone A and D into individual plastic bags and subsequently placed inside large

plastic containers to minimize atmospheric interaction. The containers were transported to the laboratory where subsamples were collected for thin sectioning. The remaining material was disaggregated by hand and stored for later use.

Flow-through columns were made using clear PVC pipe of approximately 15 cm in diameter and 25 cm in length (~4500 cm^3). Attached to the ends of each cylinder were PVC plates that contained a circular groove, to ensure a snug fit, and ports for influent or effluent flow. The base plate was permanently fixed with epoxy, while the top plate was removable and contained a compression o-ring for an airtight seal. Each column was connected to fluid and gas reservoirs with tubing. Columns were flushed with fluid from the bottom up to minimize air-filled void space, and from top to bottom with gas to facilitate the expulsion of liquid and accelerate the drying process. Preliminary experiments revealed that the waste material could be dried to ambient water saturation (~12% by wt.) within a day at a gas flushing rate of 1 L per minute.

3.3. Flow-through Experiment Procedures

Waste material from the selected horizons was packed in columns. Nylon screens (600-mesh) were placed on each end of a column to prevent mass loss. After loading, the lid was securely fastened to the column base plate by connection with metal rods and bolts. Gas-equilibrated water was pumped independently into the columns from a common reservoir at 2.5 mL min^{-1} with Barnant metering pumps. The flow rate was set to be similar to measured infiltration rates for waste at 488-DAB (Smail, pers. comm.). Depending upon the treatment, gas-equilibration of the influent was achieved by continuous sparging of the inlet reservoir with either breathing quality oxygen or zero grade nitrogen gas. Ultra purification of the nitrogen was achieved by passing the gas over hot copper in a reduction furnace prior its introduction in an experiment. Non-potable ground water pumped from a local artesian aquifer was stored in fifty-liter carboys and pre-equilibrated to the appropriate temperature and gaseous conditions before being pumped into the columns. Prior to an experimental run, each column setup

was examined for leakage, settling, and mass loss by flushing gas-equilibrated fluid through the system.

Four experimental runs were conducted sequentially, each run consisted of four independent columns that were leached for approximately 35 days. In each run, two columns contained zone A material (columns 1 and 2) and two columns contained zone D material (columns 3 and 4). In each run, columns 1 and 3 were flushed continually with fluid while columns 2 and 4 experienced a periodic wetting (5 days) and drying (2 days) cycle flow regime. Based on preliminary tests, gas flow rate was set at 1 L per minute. Flow rates were monitored and adjusted periodically during each experiment. Column experiments were conducted at two different temperatures, 12.7° and 29.4°C, to simulate winter and summer soil temperatures, respectively. Maintenance of the experimental conditions was achieved by housing the entire column set-up, including gas and liquid reservoirs, in a large environmental chamber.

The treatment sequence for the experimental runs was: 1) O_2-equilibrated fluid at 12.7° C (Run 1), 2) N_2-equilibrated fluid at 12.7°C (Run 2), 3) N_2-equilibrated fluid at 29.4°C (Run 3), and 4) O_2-equilibrated fluid at 29.4°C (Run 4). When a column experiment was initiated, effluent was collected every 4 hours for the first 48 hours, and daily thereafter. During each sampling event, effluent pH, Eh, temperature, and EC were recorded, measurements of total Fe and Fe^{2+} were performed (HACH test kit), and three samples of fluid were collected for laboratory analysis. Twenty milliliters of effluent was filtered (0.45 micron acetate syringe filter) into a glass scintillation vial preloaded with 100 microliters of trace metal grade nitric acid for dissolved metal analysis, 60 mL of unfiltered effluent was stored in an amber glass vial for measurement of acidity, and approximately 20 mL of unfiltered effluent was collected for sulfate (SO_4) analysis.

3.4. Analytical Methods

Measurements of pH, temperature, and EC were made in the environmental chamber using a HI 991301 Hanna pH meter and probe. Eh was measured separately

using an ORP probe and meter. Calibration checks were performed on all probes once per week for quality control.

Acidity titration was performed using an ABU901 autoburette and TimTalk 9 computer software. The ICP-OES analyses were performed on a Perkin-Elmer Optima 4500DV Optical Emission Spectrometer. Total Fe, Fe^{2+} and sulfate analysis were conducted using HACH test kits and a DR/890 Colorimeter. Samples for iron and sulfate determination were filtered with 0.1 micron and 0.22 micron syringe filters, respectively, prior to analysis. Geochemical modeling of aqueous-phase chemical equilibria was performed with the MINTEQA4 computer program[10]. Measured pH and Eh values were used as model inputs in the computer simulation.

Thin sections were made by Mineral Optics Laboratory (Wilder, Vermont) to determine the texture, fabric and mineralogy of zone A and D materials prior to the experiments. Percent silt and clay were determined on samples of zone A and D starting material using the hydrometer method of Gee and Bauder[11]. The XRD analyses were conducted on powder mounts of zone A and D materials prior to and at the conclusion of each experiment using a XRD diffractometer (X2 Advanced Diffraction System, Scintag Inc.) with Co Kα radiation. A TGA 2950 thermogravimetric analyzer (TA Instruments, New Castle, DE) was used for TG and DTG characterizations.

4. RESULTS AND DISCUSSION

4.1. X-Ray Diffraction and Thermal Analysis

Surficial waste material at the 488-DAB experienced fluctuating saturated/unsaturated conditions that promoted the incongruent precipitation/dissolution of minerals. During dry periods of the summer, yellow efflorescences erupting from below the surface were observed and were a common superficial feature on the basin. In addition, white globules consisting of a hard inner shell and soft outer coating with the consistency of powder were abundant in the upper 1 cm of the surface horizon. Diffraction patterns of the yellow efflorescences showed sharp peaks at 8.25, 5.45 and

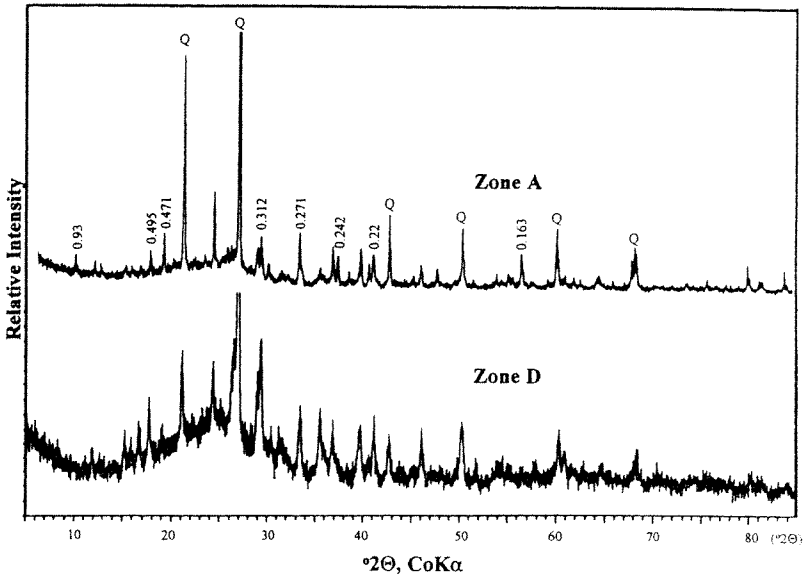

Figure 2. X-ray powder diffraction patterns of waste material from two depths in the 488-DAB.

2.76-Å, which are consistent with the iron sulfate mineral coquimbite ($Fe_2^{III}(SO_4)_3 \cdot 9H_2O$). The precipitation of iron sulfate minerals is a commonly associated product of an evaporative system that has accumulated dissolved species from pyrite oxidation[12]. As noted by Jambor et al[13], the subsequent dissolution of these salts during rain events represents an additional source of acidity and a major contributor to the contaminant pool of these systems and adjacent environments.

Two minerals associated with the white globular material were identified by XRD. Sharp diffraction peaks at 7.63, 4.28, 3.06 and 2.87- Å characteristic of gypsum ($CaSO_4 \cdot 2H_2O$) were exhibited from the external powder coating. The inner hard material showed reflections at 3.03, 2.49 and 2.28- Å, which are consistent with that of calcite ($CaCO_3$). Apparently, the acidic conditions of the basin have contributed to the dissolution of limestone particles that were co-mingled within the waste material. As with the iron salts, recrystalization of limestone as a sulfate salt likely occurred on the surface of the calcite minerals during evaporative periods.

The XRD patterns of basin material collected from zones A and D exhibited a very similar array of peaks (Figure 2). Both horizons displayed sharp peaks at 3.34, 4.25, 2.45, 2.28 and 1.81- Å, which are consistent with quartz; and at 3.12, 2.71, 2.42, 2.2 and 1.63- Å suggesting the presence of pyrite. Although it is difficult to assess due to potential peak overlap, the reflection at 4.95- Å may also suggest the presence of goethite (α-FeOOH) in samples from both horizons. Material from zone A also displayed weak reflections at 9.3, 4.71 and 3.69- Å, which is indicative of basaluminite ($Al(SO_4)(OH)_{10}$). Insoluble aluminum hydroxysulfates may precipitate from acid sulfate solutions when buffered to a relatively high pH by carbonate materials, however, a pH near 5.0 must be achieved for this to occur (pK_1 for Al-hydrolysis is 5.0[14]). Although the presence of calcite was verified in this zone, samples analyzed for pH rarely exceeded a value greater than 2.5. It is possible such minerals formed in the local environment when pH was buffer by the release of alkalinity.

Thermogravimetric (TG) analysis of zone A material displayed a weight loss of ≈ 5% between 25 and 300°C, followed by weight losses of ≈ 9 and 3% in the 400 to 500 and 750 to 900°C regions, respectively (Figure 3). Derivative thermogravimetry (DTG) indicated an inflection at 150°C, which is typical for the dehydration of gypsum[15]. Weight loss (TG) and strong DTG inflections at 450 and 500°C correspond to the oxidation of pyrite to hematite[16,17]. A broad and weak inflection at 800°C corresponding to the weight loss in the 750 to 900°C region is likely indicative of the decomposition of carbonates (calcite) and evolution of CO_2[15]. Another weak DTG inflection is exhibited at 250°C may be the result of dehydroxylation of poorly crystalline goethite, lepidocrocite, or akaganéite[18] and/or an Al-hydroxide mineral[19].

Material from zone D showed only ≈1% weight loss in the 25 to 300°C range and no significant DTG inflections. A weight loss of ≈5% occurred at the 300 to 600°C range with sharp DTG inflections at 350 and 500°C. The inflection at 350°C is likely due to the dehydroxylation of goethite[20], while the 500°C inflection is attributable to the oxidation

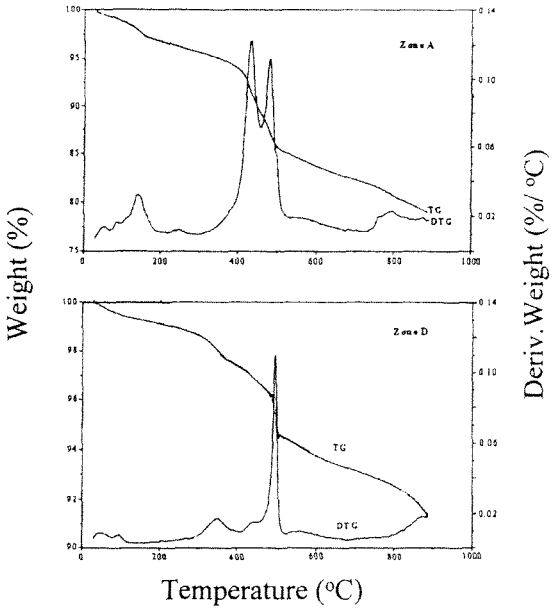

Figure 3. TG and DTG of waste material from two depths in the 488-DAB.

of pyrite to hematite as noted for zone A. Weight loss of ≈3% was observed in the 600 to 900°C region, but no significant DTG inflections were detected.

Based upon these results, it is likely that materials in the upper part of the basin are enriched to some extent with carbonate materials, while subsurface zones are primarily dominated with pyrite and secondary precipitates that resulted from its' oxidation. Apparently, gypsum precipitation is a surface phenomenon on the basin due to the relative abundance of carbonates in that zone. In addition, further evidence to support the presence of Al-hydroxides in zone A was revealed by the thermal analysis. Given that calcite was detected in zone A by both XRD and TG, the possibility for localized areas containing enough buffering potential to support a mineral such as basaluminite exists. However, gypsum and the Al-mineral phase will likely be short-lived on the 488-DAB as carbonate alkalinity is consumed over time.

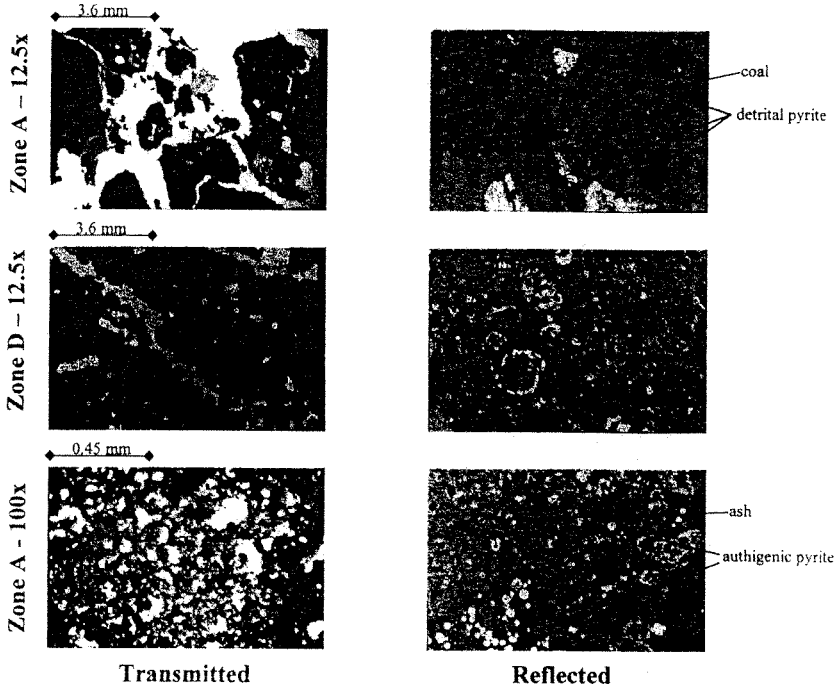

Figure 4. Thin section from zones A and D of the 488-DAB in transmitted and reflected light under 1.25x and 10.0x magnification.

Thermal analysis and XRD on samples collected from each column after the leaching procedure indicated that no major changes in mineralogy occurred during the course of the experiment.

4.2. Particle Size and Thin Section Observations

Bulk samples collected from the basin indicated that zone A and D contained 41.4 and 6.3% course fragments (>2mm diameter), respectively. Texture analysis indicated that zone A material was composed of 7.1% clay, 14.2% silt and 78.1% sand, while zone D contained 18% clay, 29.9% silt and 52.1% sand.

Thin sections of starting material for zones A and D are shown in Figure 4. Zone A contains large clasts of coal and detrital pyrite, shown as brown and brassy material in

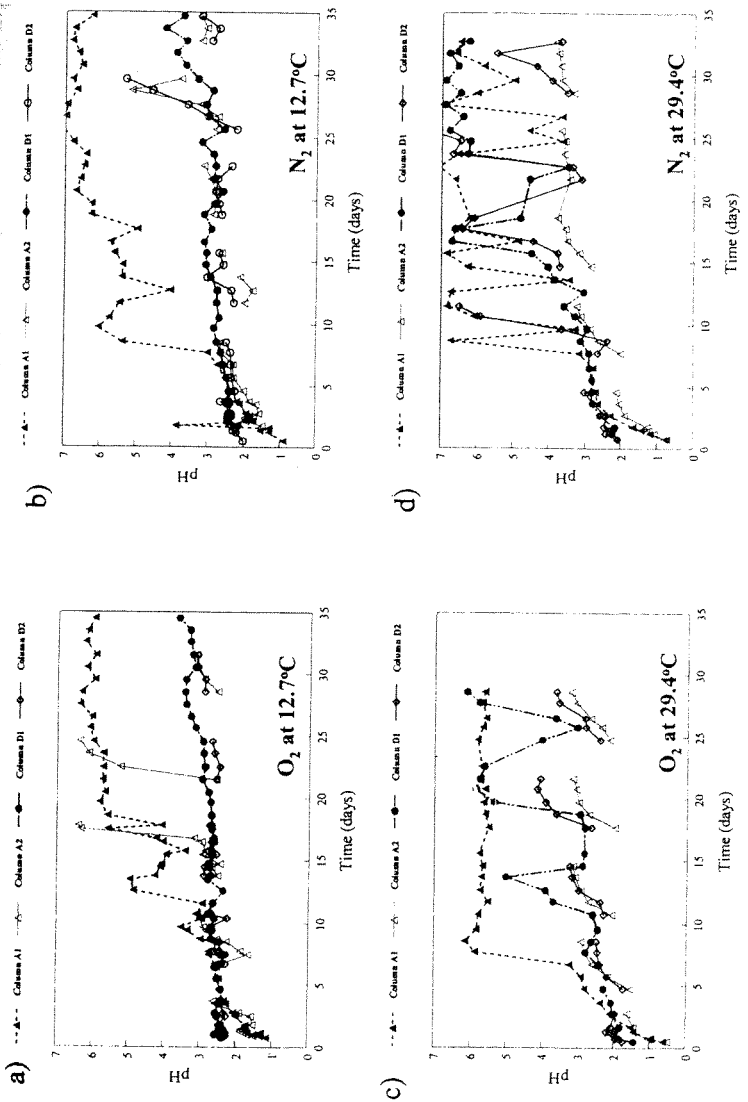

Figure 5. Effluent pH levels from zone A and D columns at (a) 12.7 ^{0}C in equilibrium with oxygen, (b) 12.7 ^{0}C in equilibrium with nitrogen, (c) 29.4 ^{0}C in equilibrium with oxygen, and (d) 29.4 ^{0}C in equilibrium with nitrogen.

reflected light, respectively, and as black grains in transmitted light. White areas in transmitted light are pore space, occasional mineral grains, or country rock.

Zone D predominantly contains fine-grained material that cannot be distinguished at relatively low magnification (12.5x). Under higher magnification (100x), a fine-grained brassy texture is noted under reflected light that is pervasive throughout the section. This material is either detrital or authigenic pyrite. At high magnification, spherical brassy grains are observed and these are most probably authigenic pyrite grains that formed through the weathering of overlying detrital pyrite grains. The circular cross-section is indicative of pyrite framboids that commonly occur in marine sediments where dissolved SO_4 diffuses into microenvironments that are slightly to strongly reducing. It is probable that pyrite was oxidized at the surface, either inorganically or through biomediated reactions, and the liberated SO_4 was transported with infiltrating waters to the subsurface where microbial Fe- and sulfate-reduction were active. Analyses are presently underway to measure $^{34}S/^{32}S$ ratios in these grains, as relatively low ratios are a strong indicator of biological sulfate reduction in terrestrial environments.

4.3 Column Eluent Chemistry

4.3.1 Eh and pH

A plot of pH over time is presented in Figure 5 for each experimental run. For column A1 (coal rubble, continuous flush), pH generally increased from ~1.0 to 6.0 over the first two weeks and then remained relatively constant thereafter. Similar low pH values (pH ~ 1 or lower) have been observed in sulfide-rich tailings impoundments and mine waste sites that have been exposed to atmospheric conditions for long periods of time[21,22]. For column A2 (coal rubble, periodic flush), pH generally increased from ~1.0 to ~2.5 within the first 3 days and increased to ~ > 3.0 by the end of the experiment. Occasional transient events were noted in the lower temperature columns where pH increased to ~6.0 over a relatively short time interval. For the fly ash residue columns (D1 and D2), effluent pH was initially higher at ~2.5 and less variable over the course of

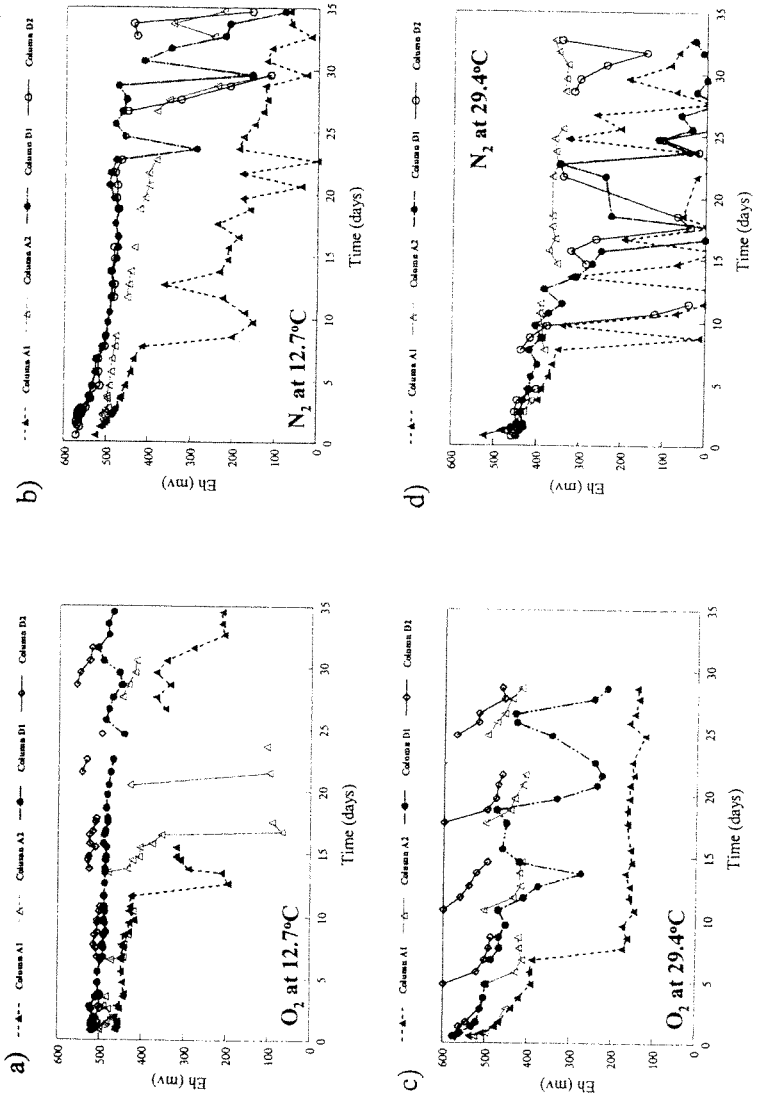

Figure 6. Effluent Eh levels from zone A and D columns at (a) 12.7 ^{0}C in equilibrium with oxygen, (b) 12.7 ^{0}C in equilibrium with nitrogen, (c) 29.4 ^{0}C in equilibrium with oxygen, and (d) 29.4 ^{0}C in equilibrium with nitrogen.

the experiments. At the low temperature, zone D effluent pH rarely exceeded ~3.0-3.5, regardless of flow regime. However, the higher temperature produced several events where the pH exceeded ~6.0 in both the oxygen and nitrogen equilibrated columns.

Effluent Eh for the column experiments are presented in Figure 6. For column A1, effluent Eh was relatively constant at ~450 mv for the first week then decreased abruptly (< 200 mv) thereafter. For column A2, effluent Eh remained relatively high at ~400-500 mv, except for several transient low Eh spikes (~100 mv) that were coincident with spikes in pH. For the fly ash residue columns (D1 and D2), effluent Eh remained relatively higher than that observed from the coal rubble material and exhibited less fluctuation for the duration of the experiments.

A general inverse correlation was observed between Eh and pH for all four experimental runs and this relationship is similar to that noted elsewhere for acid mine drainage[23,24]. The relationship between Eh and pH was consistent ($r^2 = 0.78$) both within columns of an experimental run (e.g., among flow regimes for both the coal rubble and fly ash residues) and among experimental runs (e.g., for different fluid compositions and temperatures), although slight differences in the Y-intercept were noted which could be explained by a temperature dependent reaction mechanism (Figure 7). This observation suggests that the basic chemical mechanism responsible for the production of column effluent was similar among treatments. In addition, the closeness of the curve fit between runs may suggest that the driver for pyrite oxidation in these sediments is one of a physicochemical nature rather than biological. As indicated in the introduction (equations [2] and [3]), ferric iron may act as an electron acceptor and contribute to acid production through hydrolysis and/or as a direct mechanism for pyrite oxidation. Further examination of Figure 7 reveals two dominating clusters of points; one in the pH 2 to 3 range with Eh values between 400 and 500 mv, and another in the pH 5 to 7 range with Eh values less than 200 mv. The clusters may represent the transition of iron from the Fe^{3+} valence state (low pH, high Eh) to the Fe^{2+} state (circumneutral pH, low Eh). With

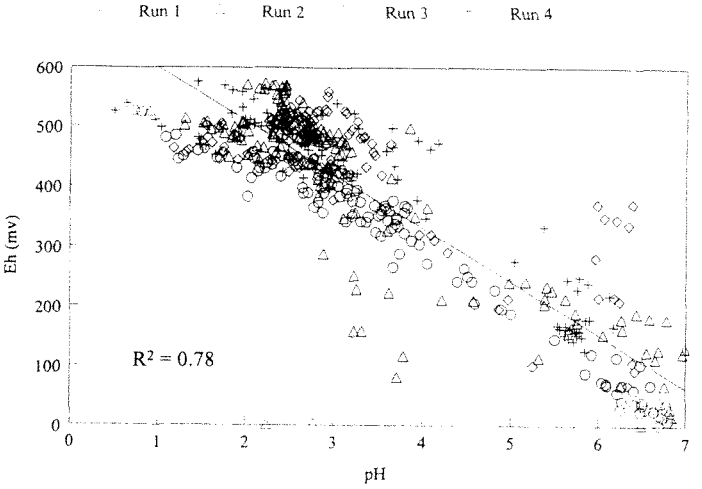

Figure 7. Relationship between pH and Eh in column effluents.

the removal of ferric iron from the system (via reduction or precipitation) acid generation and potential pyrite oxidation is lowered and waters make the transition from acidic to circumneutral.

4.3.2 Major Element Composition

The discharge of sulfur from column A1 exhibited similar patterns throughout the experiment, regardless of the temperature or gas phase (Figures 8 – 11). In general, the S content gradually fell from an initial concentration near 10,000 mg L^{-1} to 100 mg L^{-1} after one week of flushing. Subsequent effluent S concentrations remained relatively flat between 100 mg L^{-1} and 50 mg L^{-1}. Systematic decreases were observed in individual flushing cycles of runs that experienced periodic wetting and drying conditions and this was consistent with the pH-Eh data. Peaks and valleys observed in continuously flushed columns may be indicative of the highly reactive material of the basin, but could also be attributable to changes in the solution flow path within the column. Sulfur concentrations from D1 eluents (all runs) followed the same pattern as those described for column A1 except that the initial concentrations were significantly lower in the deeper horizon

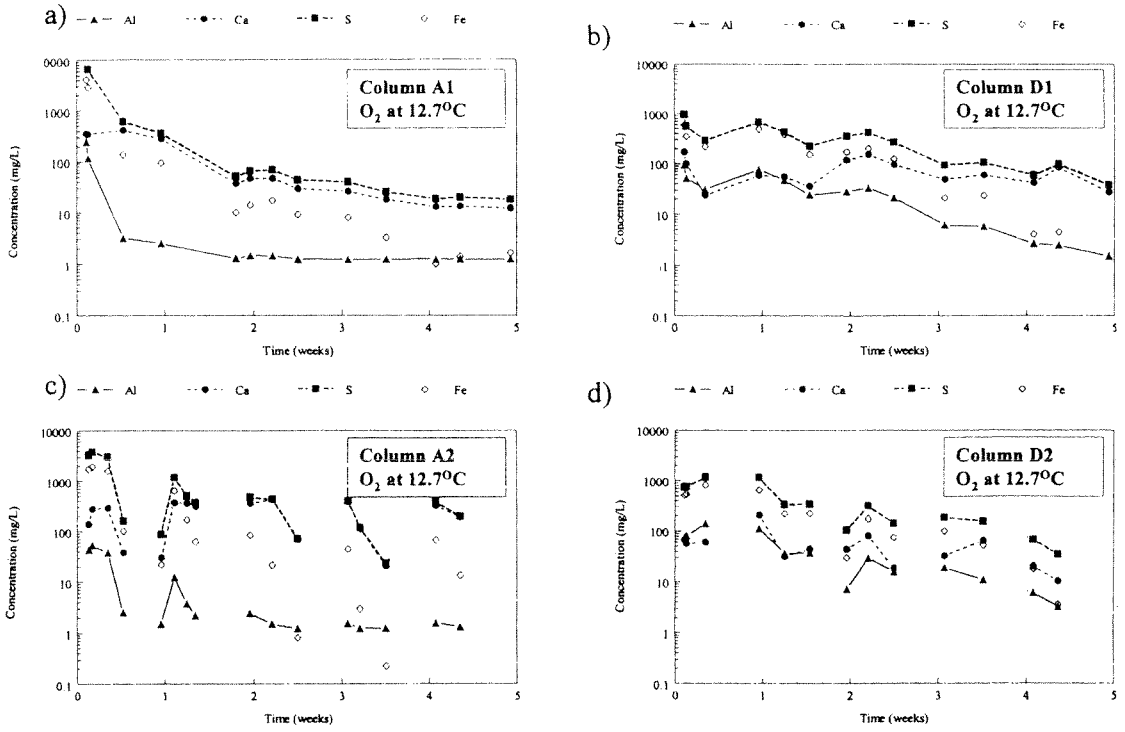

Figure 8. Major elemental composition of effluents from (a) continuously flushed zone A material, (b) continuously flushed zone D material, (c) episodically flushed zone A material, and (d) episodically flushed zone D material in equilibrium with oxygen at 12.7°C.

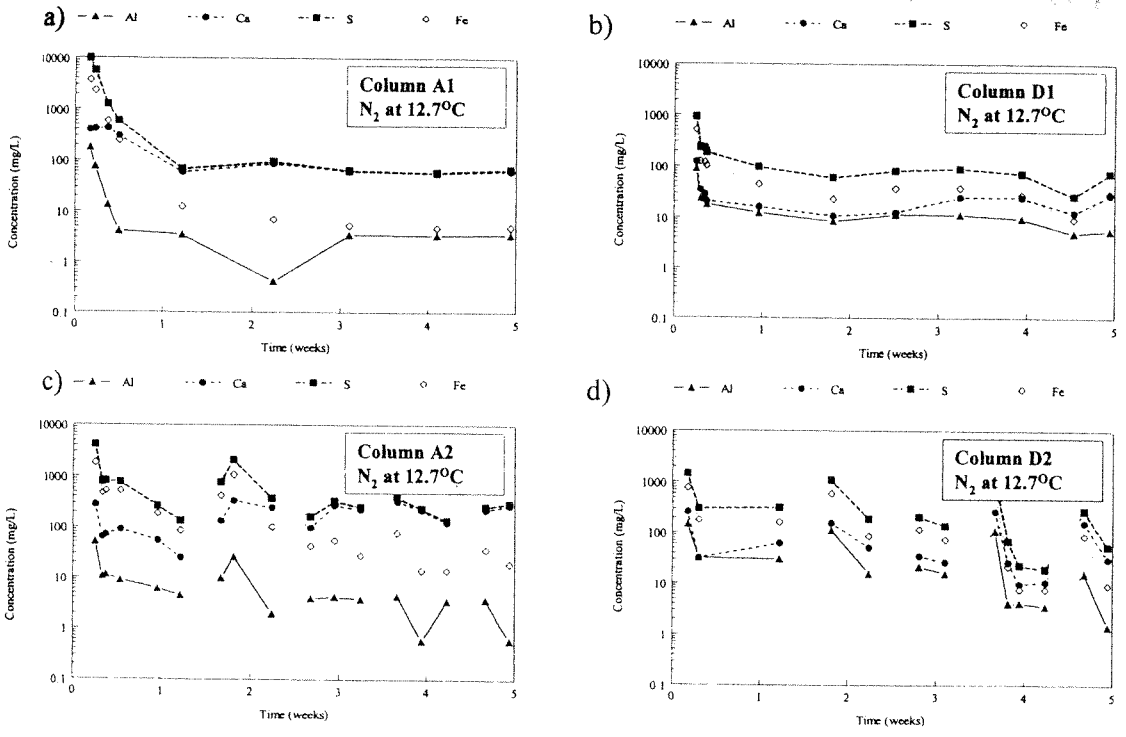

Figure 9. Major elemental composition of effluents from (a) continuously flushed zone A material, (b) continuously flushed zone D material, (c) episodically flushed zone A material, and (d) episodically flushed zone D material in equilibrium with nitrogen at 12.7°C.

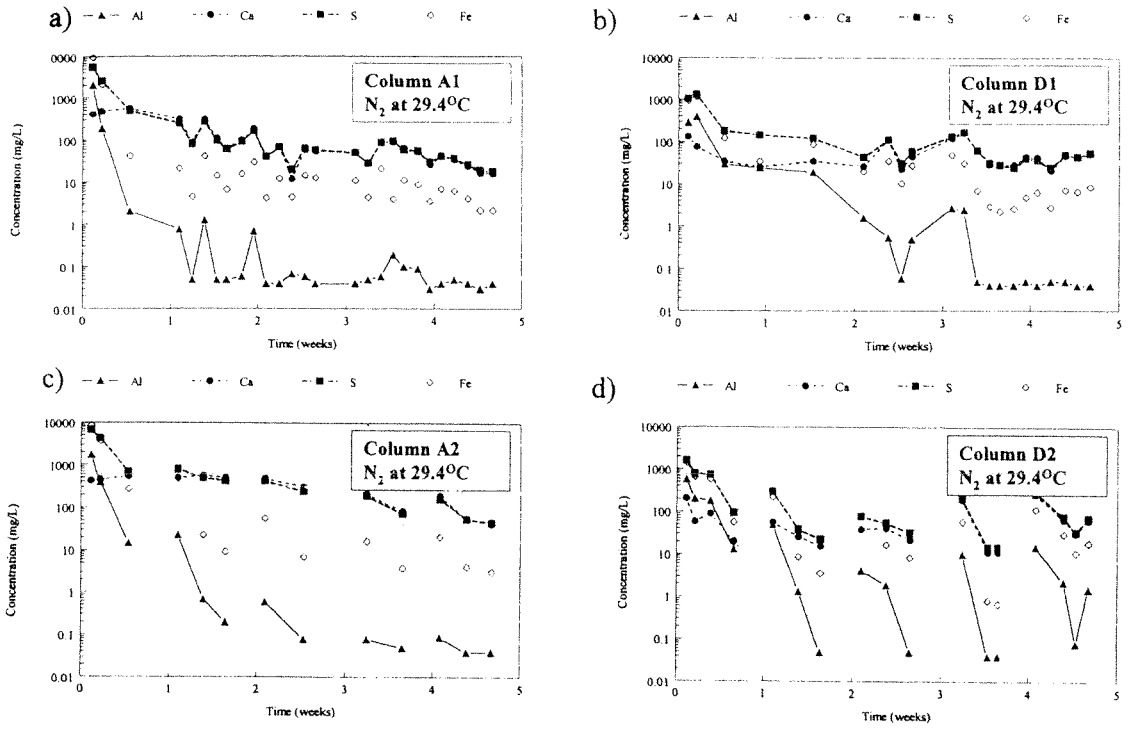

Figure 10. Major elemental composition of effluents from (a) continuously flushed zone A material, (b) continuously flushed zone D material, (c) episodically flushed zone A material, and (d) episodically flushed zone D material in equilibrium with nitrogen at 29.4^{0}C.

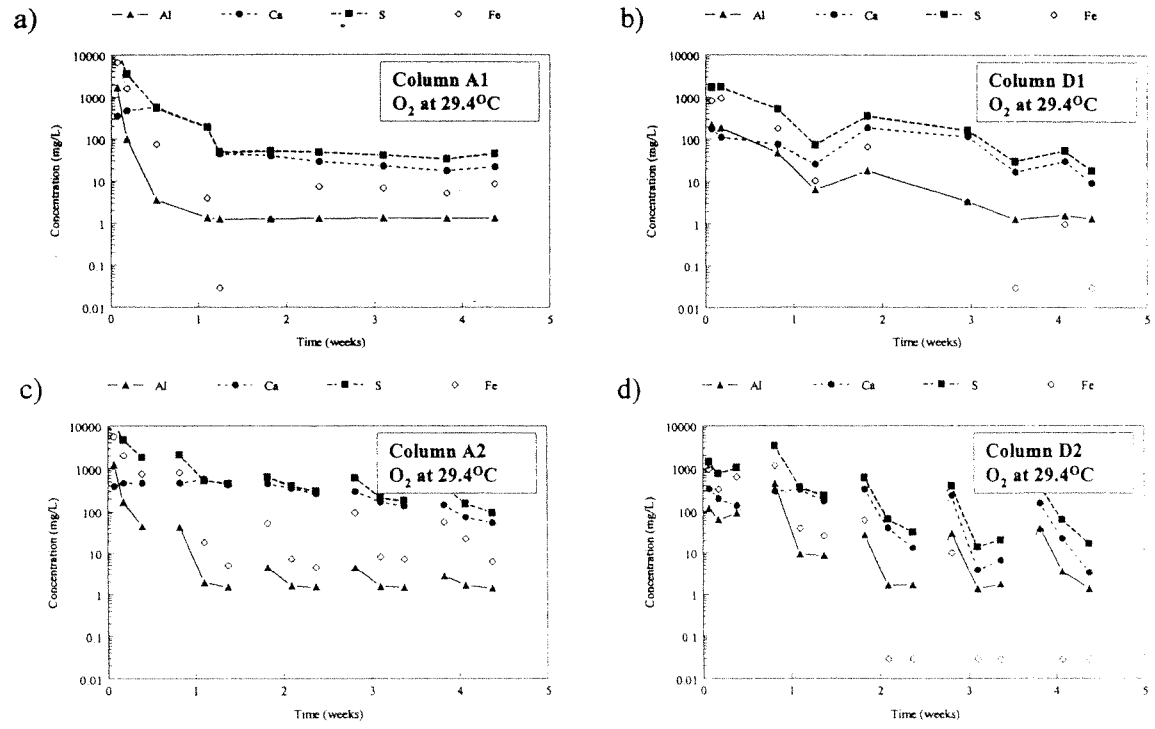

Figure 11. Major elemental composition of effluents from (a) continuously flushed zone A material, (b) continuously flushed zone D material, (c) episodically flushed zone A material, and (d) episodically flushed zone D material in equilibrium with oxygen at 29.4^{0}C.

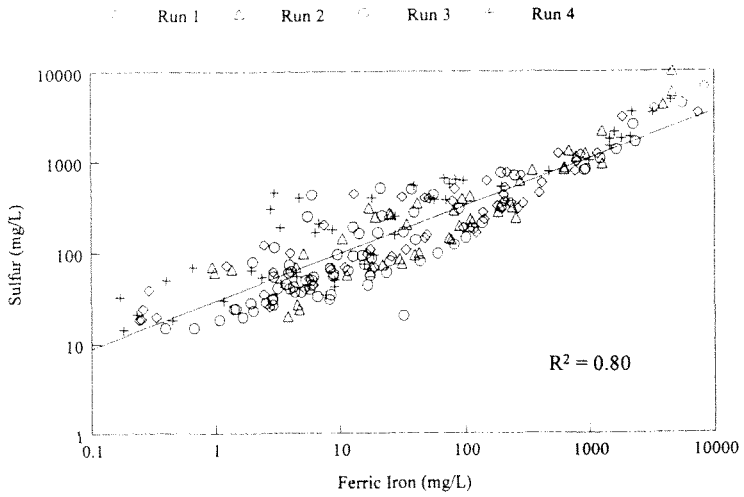

Figure 12. Relationship between sulfur and ferric iron in column effluents.

material (1,000 vs. 10,000 mg L^{-1}). The higher initial S content in the column A1 material is likely a result of the dissolution of evaporative salts that formed on the basin's surface. The episodic wetting and drying in columns A2 and D2 showed the same general downward trend in S levels with time, however, concentrations tended to exhibit a "rebound" effect after each successive dry-down period. The magnitude of this "rebound" differed slightly among columns and between runs, but the general result was similar in that the S concentrations at the beginning and end of a wetting cycle were lower than that of the preceding cycle. Even though the pH of these episodic events reached levels above 6.0 toward the end of a cycle, the pH value at the beginning of a cycle rarely exceeded a level of 3.0 for both columns (A2 and D2) during all runs (Figure 5). As such, mobility of the elements was highest at the beginning of a cycle.

Initial calcium concentrations in effluents were $\leq$ 400 mg L^{-1} for all runs. By the end of week 1, Ca concentrations from zone A columns dropped to levels similar to that of S and tracked S concentration thereafter. In zone D columns, S approached Ca by the end of the experiment. The approach was kinetically favored at the higher temperature.

The strong association between Ca and S suggests that these elemental concentrations may be controlled by the solubility of a solid or mineral of similar stoichiometry, most probably gypsum[25]. The episodic flushing of column D2 yielded a Ca "rebound" effect similar to that of column A2.

Iron concentrations for column A1 eluents were near 10,000 mg L^{-1} at the beginning of each experimental run, and rapidly fell to levels approaching 10 mg L^{-1} by the end of the first week. Subsequent effluent Fe concentrations remained in the 1 to 10 mg L^{-1} range. Although lower in concentration, column A1 elution curves for Fe maintained a similar pattern to that observed for S and Ca for all runs. Column D1 eluents were similar to that of A1 for all runs. Once again, the eluent pattern for the columns experiencing episodic wetting exhibited a "rebound" effect, and mimicked that of sulfur. A plot of ferric iron (Fe^{3+}) vs. sulfur resulted in a positive correlation ($r^2 = 0.80$) for all four experimental runs (Figure 12). This observation reemphasizes the possibility that a basic chemical mechanism responsible for the production of column eluent was similar among all treatments. In addition, the closeness of the curve fit between runs may suggest that Fe^{3+} is the principal oxidizing agent leading to the formation of AD from the 488-DAB material. As such, maintenance of the iron redox couple at a level favoring the ferrous state (~ < 150 mv) may be an essential factor for the control of pyrite oxidation in these sediments.

Initial eluent aluminum concentrations for column A1 were less than 300 mg L^{-1} for runs 1 and 2 (Figures 8a and 9a), and greater than 1,000 mg L^{-1} for runs 3 and 4 (Figures 10a and 11a). The difference between the concentration levels is most likely attributable to initial pH conditions of the runs. The warmer runs (3 and 4) produced a more acidic initial solution (~0.3 pH units lower), which likely increased the solubility of aluminum in those columns. By the end of the first week, A1 columns generally exhibited an eluent pH > 4.0 (Figure 5) and aluminum concentrations were $\leq$ 1.0 mg L^{-1}. Runs 1, 2 and 4 for column A1 maintained an eluent concentration around 1.0 mg L^{-1} for the

duration of the experiment, however, run 3 (N_2 at 29.4°C) exhibited a further decrease to ~ 0.05 mg L^{-1} (Figure 10a). We suspect that the lower aluminum concentration in run 3 is attributable to enhanced microbial metabolism under anaerobic conditions, which resulted in a higher pH within the column and enhanced Al precipitation.

4.3.3 Trace Element Composition

Examination of the trace element data from ICP analysis revealed four elements (As, Cu, Se, and Zn) with appreciable quantities in the eluent samples. Graphs depicting the change in concentration of these elements over the course of the experiment are presented in Figures 13 –16. The concentration of zinc was relatively stable during the experiment regardless of the temperature, gas phase, or column material. Zinc concentrations fluctuated from 1 mg L^{-1} at the beginning of a run to ~ 0.1 mg L^{-1} at the end. The rebound effect observed with the major elements did occur for Zn in columns A2 and D2.

Copper concentration in columns A1 and D1 follows a similar pattern to that of zinc during the first week, but concentrations tend to decline further to the 0.01 mg L^{-1} level through the remainder of the experiment. The "rebound" of copper is exhibited in episodically flushed column A2 when oxygen is present (Figures 13c and 16c), however, the response does not occur in the presence of nitrogen (Figures 14c and 15c). In addition, the final effluent concentration in the A2 column is generally lower when leached in the more reducing N_2 environment. Column D2, on the other hand, exhibits the rebound for all runs but is more expressed at the higher temperature with a general order of magnitude change in concentration during each solution pulse phase. This suggest that a slight reduction in the water oxidation state may deter Cu leaching from the zone A coal rubble material, whereas continual Cu releases from the zone D ash zone are likely to continue with each successive wet/dry period.

Selenium concentrations in runs 2 through 4 were below detection for columns A1 and D1 after one week of continual leaching (Figures 14a,b-16a,b), while in run 1 (O_2

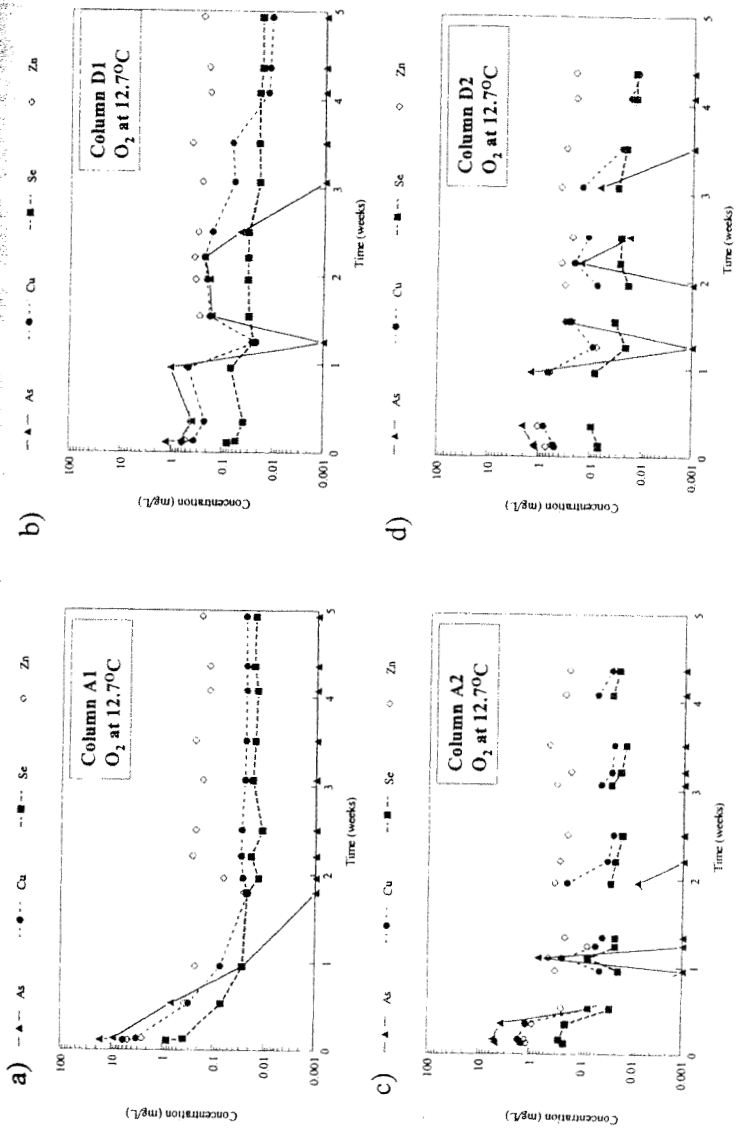

Figure 13. Minor elemental composition of effluents from (a) continuously flushed zone A material, (b) continuously flushed zone D material, (c) episodically flushed zone A material, and (d) episodically flushed zone D material in equilibrium with oxygen at 12.7°C.

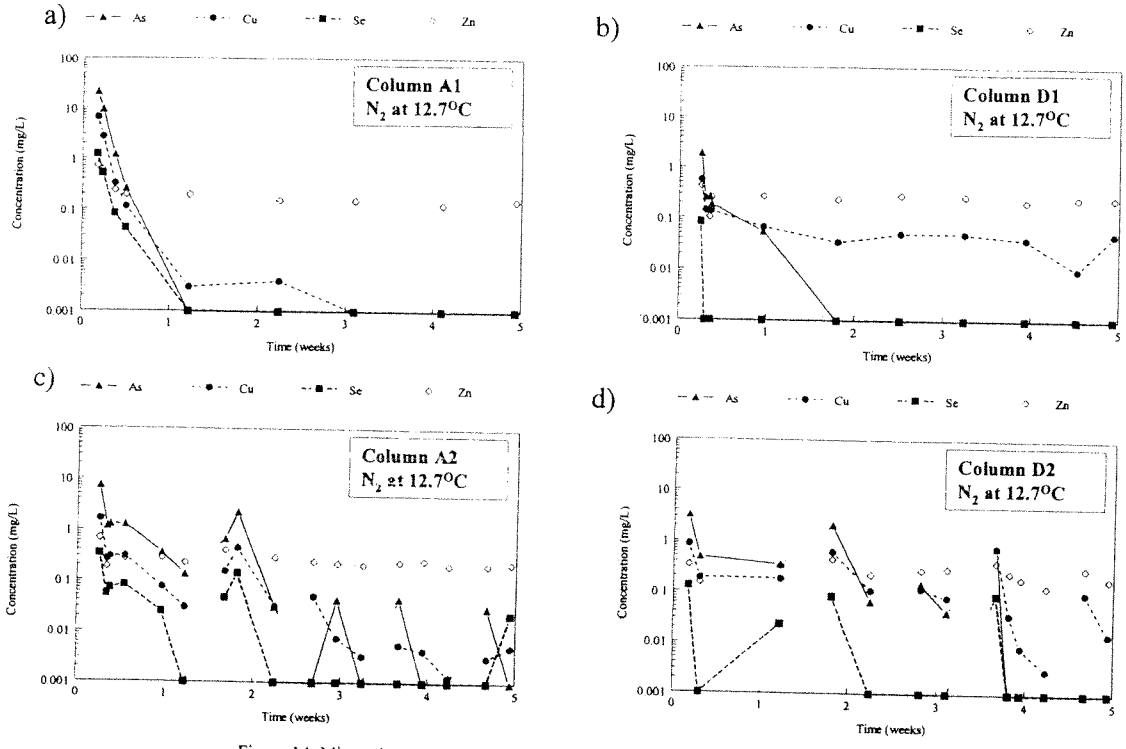

Figure 14. Minor elemental composition of effluents from (a) continuously flushed zone A material, (b) continuously flushed zone D material, (c) episodically flushed zone A material, and (d) episodically flushed zone D material in equilibrium with nitrogen at 12.7°C.

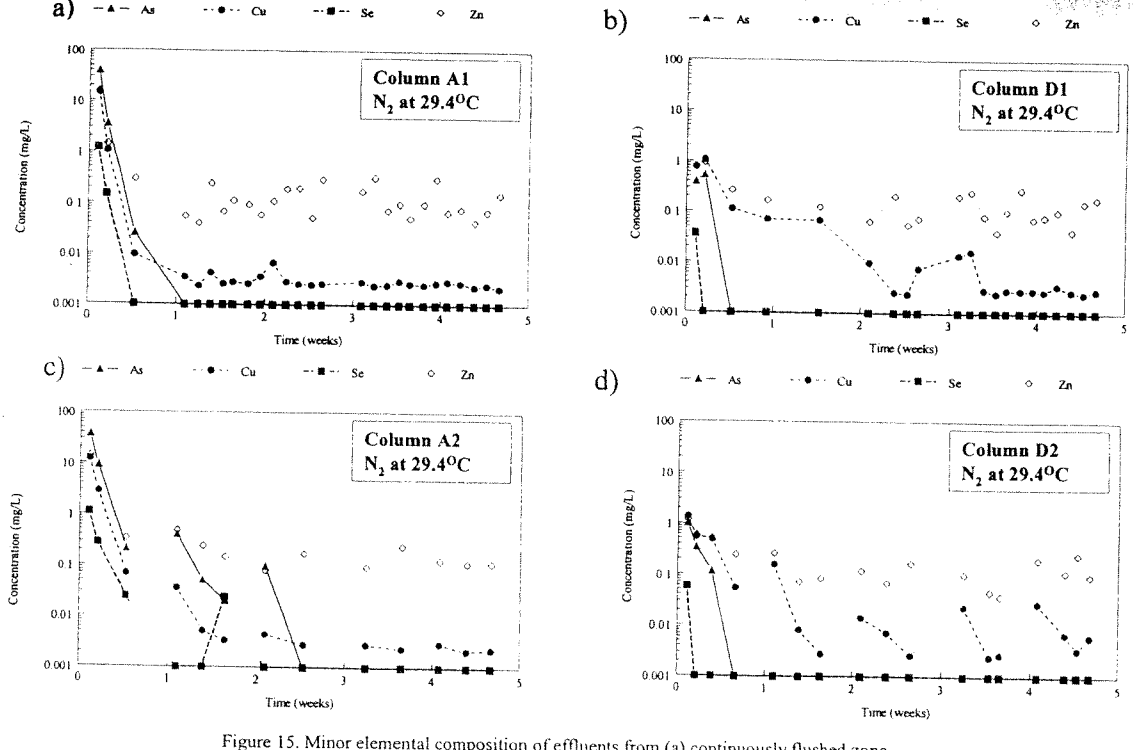

Figure 15. Minor elemental composition of effluents from (a) continuously flushed zone A material, (b) continuously flushed zone D material, (c) episodically flushed zone A material, and (d) episodically flushed zone D material in equilibrium with nitrogen at 29.4°C.

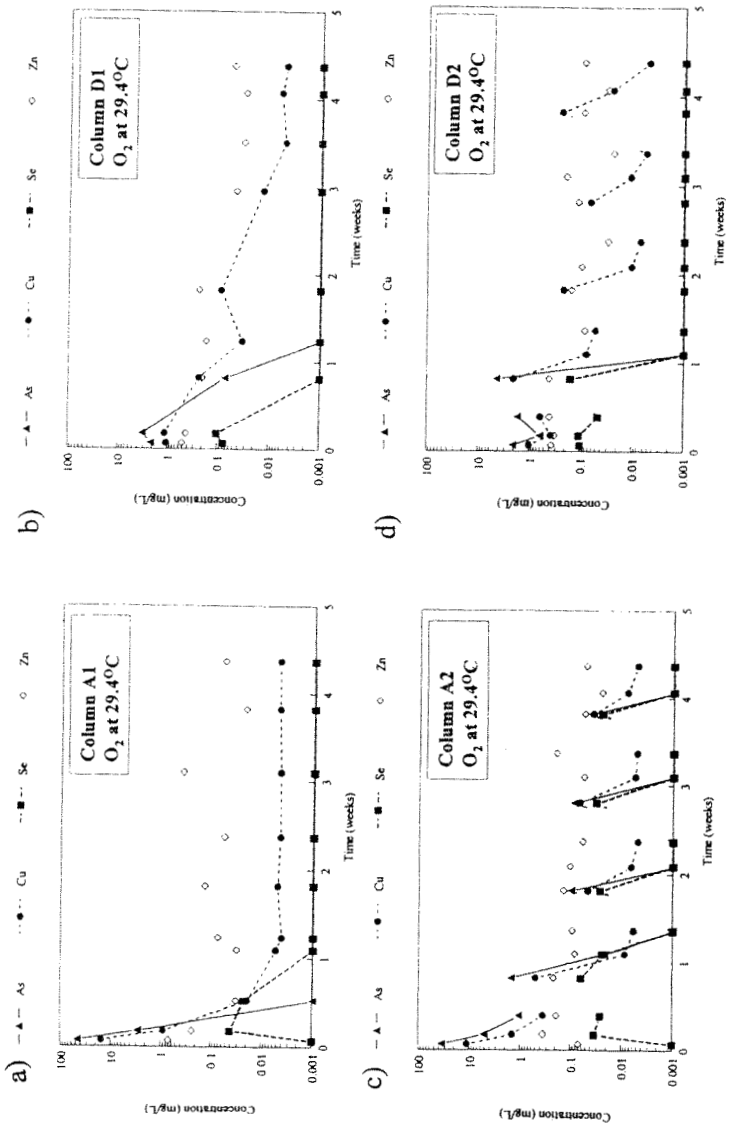

Figure 16. Minor elemental composition of effluents from (a) continuously flushed zone A material, (b) continuously flushed zone D material, (c) episodically flushed zone A material, and (d) episodically flushed zone D material in equilibrium with oxygen at 29.4°C.

at 12.7°C) Se concentrations were slightly above detection ~ 0.03 mg L^{-1} in both columns (Figure 13a,b). Selenium mobility in soils is controlled by pH and redox conditions[26], but the difference between these factors over the four runs was not significant enough to elicit the observed response. Relationships to other chemical constituents that may explain the Se behavior in run 1 were not observed. As such, the enhanced Se mobility was probably due to a mobile Se-colloidal fraction that formed under the specific environmental conditions of this run. Selenium concentration in the eluents from episodic flushing (columns A2 and D2) in the presence of N_2 (Figures 14c,d and 15c,d) did not differ significantly from that in the saturated columns. Some fluctuation in Se concentration was observed in the lower temperature run during episodic flushing (Figure 14), however, a "rebound" was not observed for all pulses. The episodically flushed columns saturated with oxygen at a low temperature exhibited a nearly identical pattern to those described for the saturated columns in run 1 (Figure 13). Once again, concentration levels did not fall below ~ 0.03 mg L^{-1}, and the rebound between pulses were minimal during this run. At the higher temperature, the rebound was clearly evident in the zone A coal rubble column (A2) (Figure 16c) but missing in the deeper zone D ash column (D2) (Figure 16d).

Arsenic showed a very similar pattern to that described for selenium. Initial As concentrations were > 10 mg L^{-1} and ~ 1 mg L^{-1} in zones A and D, respectively. In the saturated columns, As concentrations fell below detection after one week of leaching for all runs. Arsenic in the episodically flushed columns exhibited a wide array of responses with changes in environmental conditions. At low temperature, eluted As was below detection in zone A materials within two weeks of leaching in the presence of O_2 (Figure 13c), but exhibited a rebound to levels of ~ 0.03 mg L^{-1} with each successive pulse in the presence of N_2 (Figure 14c). Eluent As concentrations from zone D1 materials at this temperature were below detection by week four regardless of the gas phase (Figures 13d and 14d). Conversely, the higher temperature elicited quite a different response. Eluent

As levels from the zone D2 columns (N_2 and O_2) were below detection by the second pulse phase of the run (Figures 15d and 16d). In the zone A1 columns under higher temperature, As concentrations eventually fell below detection during week 2 in the presence of N_2 (Figure 15c), but were maintained well above detection with each successive pulse in the presence of O_2 (Figure 16c).

The response of As and Se in zone A under the presence of the differing gases at the higher temperature (Figures 15 and 16) is very informative from the standpoint of evaluating the usefulness of a cover for controlling AD release. For demonstration purposes, we may assume that these two runs represent the ambient state of the 488-DAB basin during the summer. Under saturated conditions there would be essentially no release of these toxic substances from the surface materials once an initial pulse of fluid has migrated through the subsurface. This initial contaminant pulse is probably attributable to the dissolution of evaporative salts. Under the changing conditions associated with intermittent rains at 488-DAB, the pulse is reestablished through each successive wet/dry period. As such, the waste is a long-term source of potential contamination via evaporation and precipitation. However, if there were a slight reduction in the oxidation state of water that comes in contact with the coal rubble material (e.g. N_2 column experiments) Se and As mobility would be inhibited. The use of a cover, particularly one enriched with organic matter, could generate this response. Not only would the cover provide a buffer against direct exposure to the oxidizing forces of water and air, but microbial oxygen demand within the cover could also result in lowering the oxidizing potential of rainwater prior to contact with the waste material.

4.4 Mineral Solubility

The solution saturation indices (SI) of the column eluents with respect to various minerals were evaluated using the equilibrium geochemical speciation model MINTEQA2[10]. The SI (logQ/K), where Q = ion activity product and K = solubility product constant, was calculated for each column after one and four weeks of leaching

(Tables 1 and 2). A SI of zero indicates equilibrium, a negative value undersaturation, and a positive value supersaturation. At one week of leaching most columns were undersaturated with respect to the various minerals examined (Table 1). The column A1, during run 2 (N_2 at 12.7°C), was the only example of a run containing eluents that were supersaturated with respect to more than one mineral. The precipitation of basaluminite, jurbanite ($Al(OH)SO_4$), boehmite (γ-AlOOH), diaspore (χ-ALOOH), gibbsite ($Al(OH)_3$), goethite, hematite (χ-Fe_2O_3), lepidocrocite, magnetite (Fe_3O_4), and possibly an amorphous $Al(OH)_3$ may have occurred in this column due to high pH (6.0) conditions that were not achieved by any other run or column at this stage of the experiment. Hematite was also exhibited at or above saturation in many other columns and runs. Gypsum, anhydrite ($CaSO_4$) and jurbanite were close to equilibrium in several columns during various runs.

After four weeks of leaching, column A1 exhibited tremendous changes in its SI for all runs. In this column, most of the eluent solutions were either at equilibrium or supersaturated with respect to the Al and Fe oxide, hydroxide and hydroxysulfate minerals modeled (Table 2). This correlates well with the high pH conditions observed for column A1 at four weeks. With the exception of run 3 (N_2 at 29.4°C), however, SI's for column D1 did not change significantly after four weeks of leaching. Once again, this correlates well with the pH values at that point in time (Figure 5). The experimental conditions of run 3 resulted in pH levels that were sustained above 6.0 in column D1, thus allowing for the potential precipitation of various Fe and Al minerals. The episodic flushing of columns A2 and D2 resulted in lower pH values and higher element concentrations at four weeks than that observed in the constantly saturated columns. As such, the saturation indices did not change greatly through the course of the experiment. A slight enrichment in SI was observed at four weeks for the iron minerals goethite, lepidocrocite, magnetite and hematite for column D2 during run 1 (O_2 at 12.7°C). Saturation indices for pyrite remained highly unsaturated throughout the course of the

Table 1. Saturation indices (log Q/K)† of column effluents for selected minerals after one week of leaching.

Column§	A1				A2				D1				D2			
Treatment†	1	2	3	4	1	2	3	4	1	2	3	4	1	2	3	4
Mineral																
$Al(OH)_3$ (a)	-8.98	-0.13	-6.65	-6.02	-9.19	-8.19	-8.94	-7.92	-7.96	-7.85	-5.78	-6.35	-8.40	-8.06	-6.44	-7.78
Basaluminite	-19.27	9.89	-15.38	-13.31	-20.31	-16.59	-21.96	-19.54	-14.96	-15.49	-11.80	-14.41	-16.48	-15.65	-13.54	-18.61
Jurbanite	-1.56	1.02	-1.53	-1.18	-1.93	-1.26	-1.32	-1.73	-0.26	-0.98	-0.35	-1.08	-0.27	-0.58	-0.27	-1.24
Alunite	-24.69	-24.10	-24.41	-23.40	-25.07	-23.14	-19.55	-23.25	-20.36	-21.76	-19.92	-21.25	-20.13	-20.86	-19.87	-21.11
Anhydrite	-0.64	-1.75	-0.57	-0.81	-2.59	-1.89	-0.36	-0.32	-1.34	-2.18	-1.77	-2.00	-0.70	-1.33	-1.33	-0.61
Boehmite	-6.81	2.03	-4.42	-3.79	-7.03	-6.02	-6.71	-5.68	-5.79	-5.68	-3.55	-4.12	-6.23	-5.89	-4.21	-5.55
Diaspore	-4.98	3.86	-2.73	-2.11	-5.20	-4.20	-5.02	-4.00	-3.97	-3.86	-1.87	-2.43	-4.41	-4.07	-2.52	-3.86
Ferrihydrite	-4.64	-1.42	-4.47	-4.00	-4.88	-3.81	-5.32	-4.69	-3.85	-3.45	-4.15	-3.41	-4.16	-3.60	-3.60	-3.70
Gibbsite	-5.87	2.97	-3.60	-2.97	-6.08	-5.08	-5.89	-4.87	-4.85	-4.74	-2.73	-3.30	-5.29	-4.95	-3.39	-4.73
Goethite	-1.83	1.38	-1.79	-1.32	-2.07	-1.01	-2.63	-2.01	-1.04	-0.66	-1.47	-0.72	-1.36	-0.79	-0.92	-1.02
Gypsum	-0.33	-1.44	-0.33	-0.57	-1.50	-1.57	-0.11	-0.09	-1.02	-1.87	-1.54	-1.76	-0.39	-1.02	-1.09	-0.37
Hematite	-1.33	5.10	-1.17	-0.23	-1.81	0.31	-2.85	-1.61	0.24	1.01	-0.53	0.95	-0.39	0.73	0.56	0.35
H-Jarosite	-7.40	-10.29	-9.34	-8.35	-8.42	-5.93	-6.91	-7.75	-4.43	-4.82	-7.59	-5.76	-4.40	-4.09	-4.58	-4.10
Lepidocrocite	-2.21	1.01	-2.73	-2.29	-2.45	-1.38	-3.56	-2.98	-1.42	-1.07	-2.45	-1.69	-1.78	-1.19	-1.87	-1.99
Maghemite	-8.06	-1.62	-9.11	-8.23	-8.55	-6.41	-10.76	-9.61	-6.50	-5.78	-8.56	-7.03	-7.20	-6.03	-7.36	-7.63
Magnetite	-4.80	6.38	-3.38	-2.70	-5.87	-2.91	-6.19	-4.55	-3.06	-2.57	-2.98	-1.77	-3.73	-14.92	-1.69	-2.86
FeS (ppt.)	-52.80	-42.06	-42.51	-48.77	-56.31	-57.69	-43.44	-46.17	-57.32	-63.93	-46.69	-55.44	-54.54	-59.40	-48.81	-56.25
Pyrite	-73.34	-59.66	-56.81	-67.65	-79.08	-82.19	-56.98	-62.40	-81.29	-92.84	-63.88	-78.97	-76.30	-85.00	-67.54	-79.74

†Positive values indicate supersaturation and negative values undersaturation; Q = ion activity product; K = solubility constant.

‡Treatment 1 = O_2-equilibrated at 12.7^0 C; 2 = N_2-equilibrated at 12.7^0 C; 3 = N_2-equilibrated at 29.4^0 C; 4 = O_2-equilibrated at 29.4^0 C.

§Columns A1 and D1 received continuous wetting; columns A2 and D2 received periodic wetting.

Table 2. Saturation indices (log Q/K)† of column effluents for selected minerals after four weeks of leaching.

Column§	A1				A2				D1				D2			
Treatment†	1	2	3	4	1	2	3	4	1	2	3	4	1	2	3	4
Mineral																
$Al(OH)_3$ (a)	1.16	1.74	-0.76	0.42	-9.18	-7.44	-6.94	-7.49	-5.97	-6.38	-0.96	-4.34	-7.16	-6.83	-6.30	-6.39
Basaluminite	12.70	14.86	1.85	7.24	-20.18	-14.85	-17.04	-18.22	-9.43	-10.80	-0.82	-7.83	-13.22	-12.52	-15.44	-14.52
Jurbanite	0.04	0.39	-1.89	-0.115	-1.79	-1.56	-2.30	-1.71	-0.67	-0.60	-3.91	-0.82	-0.86	-1.01	-2.57	-1.31
Alunite	-30.05	-29.93	-33.26	-26.49	-25.26	-26.3	-26.61	-22.94	-24.23	-22.00	-41.58	-22.97	-23.16	-23.67	-28.09	-21.87
Anhydrite	-2.66	-1.66	-1.76	-2.19	-0.61	-0.83	-0.86	-1.35	-1.63	-2.03	-1.78	-1.94	-1.99	-2.04	-1.88	-2.12
Boehmite	3.33	3.91	1.46	2.64	-7.02	-5.27	-4.71	-5.26	-3.80	-4.20	1.26	-2.11	-4.99	-4.66	-4.07	-4.16
Diaspore	5.15	5.73	3.15	4.33	-5.19	-3.45	-3.02	-3.58	-1.98	-2.39	2.94	-0.42	-3.17	-2.84	-2.38	-2.48
Ferrihydrite	2.17	0.36	-0.86	-0.46	-4.81	-4.83	-4.09	-3.78	-3.17	-3.34	-0.04	-1.94	-2.19	-3.58	-4.30	-3.39
Gibbsite	4.27	4.85	2.28	3.47	-6.07	-4.33	-3.89	-4.44	-2.86	-3.27	2.08	-1.29	-4.05	-3.73	-3.25	-3.34
Goethite	4.98	3.17	1.82	2.22	-2.00	-2.03	-1.41	-1.10	-0.36	-0.55	2.63	0.73	0.61	-0.78	-1.62	-0.71
Gypsum	-2.35	-1.35	-1.52	-1.95	-0.29	-0.51	-0.62	-1.12	-1.32	-1.72	-1.55	-1.70	-1.68	-1.72	-1.64	-1.88
Hematite	12.30	8.68	6.05	6.85	-1.68	-1.72	-0.41	0.19	1.60	1.23	7.68	3.88	3.56	0.76	-0.83	0.98
H-Jarosite	-3.97	-9.19	-10.93	-8.59	-7.93	-10.92	-9.14	-5.84	-7.17	-6.59	-12.07	-4.88	-2.20	-7.26	-11.55	-6.07
Lepidocrocite	4.59	2.79	0.86	1.27	-2.39	-2.44	-2.35	-2.07	-0.76	-0.98	1.66	-0.22	0.21	-1.20	-2.58	-1.68
Maghemite	5.54	1.95	-1.91	-1.09	-8.43	-8.53	-8.35	-7.79	-5.16	-5.61	-0.30	-4.09	-3.21	-6.05	-8.80	-7.01
Magnetite	13.87	11.79	9.25	9.62	-5.34	-4.40	-2.22	-2.66	-1.31	-1.53	12.48	2.32	0.24	-2.16	-2.66	-2.63
FeS (ppt.)	-70.41	-42.32	-28.89	-35.37	-53.16	-45.50	-42.43	-53.09	-61.63	-58.29	-22.75	-58.33	-72.05	-57.74	-41.72	-63.72
Pyrite	-110.07	-62.12	-38.59	-49.47	-73.82	-61.54	-57.10	-74.67	-89.74	-83.87	-29.51	-85.39	-97.42	-82.78	-56.06	-92.89

†Positive values indicate supersaturation and negative values undersaturation; Q = ion activity product; K = solubility constant.

‡Treatment 1 = O_2-equilibrated at 12.7^0 C; 2 = N_2-equilibrated at 12.7^0 C; 3 = N_2-equilibrated at 29.4^0 C; 4 = O_2-equilibrated at 29.4^0 C.

§Columns A1 and D1 received continuous wetting; columns A2 and D2 received periodic wetting.

experiment. Given the redox conditions of the experiment (Figure 6), the re-precipitation of pyrite or formation of metal sulfides was not anticipated and was not considered as a pathway for metal retention in the columns during the flow-through experiments.

5. CONCLUSIONS

In an effort to evaluate remedial options for an abandoned fly ash/ reject coal landfill, a laboratory column experiment was conducted to characterize the geochemistry of the waste material and associated lechate under differing environmental conditions. Columns were generated using materials from the surface of the landfill, primarily coal rubble, and those found deeper in the profile, primarily fly ash residue. The coal rubble zone contained large clasts of coal and detrital pyrite, secondary iron and aluminum precipitates, and evaporative iron-sulfate and calcium-sulfate salts, which formed from the weathering of pyrite and dissolution of carbonates. The iron-sulfate salts (coquimbite) represent a significant source of acidity on the landfill. The fly ash zone contained authigenic pyrite framboids that were likely formed through the weathering of the overlying detrital pyrite fragments, and secondary iron precipitates. Because of their dissimilar compositions, the two materials responded differently to the environmental conditions of the flow-through experiment.

Initial eluents from the coal rubble zone columns (zone A) were substantially lower in pH ($\sim \leq 1.0$) than that from the fly ash columns, regardless of temperature or flow regime. In continuous flowing (saturated) columns, the pH of fluids from the coal rubble zone established a dynamic equilibrium at a pH of 6 to 7 within the first week of the experiment, whereas eluent pH from the fly ash zone fluctuated more erratically from low to high. Eluent pH also increased consistently within columns that were episodically flushed; regardless of the temperature or flow regime, although the long-term increase in pH was significantly lower than that observed in the continuous flow experiments. A temperature effect on acidity was exhibited in the fly ash columns. At 12.7^{0}C, effluent chemistry was not affected greatly by gas composition or flow regime, and pH generally

did not increase above 3.5. However, eluent pH increased both episodically and periodically at 29.4^{0}C, suggesting that reactive surfaces were partially stabilized and inorganic salts were effectively mobilized from the system. This effect was more pronounced in columns that were exposed to nitrogen compared to those exposed to oxygen.

As with the pH response, initial concentrations of major and minor elements were substantially higher in the coal rubble effluents than the fly ash zone. However, concentration ranges were similar between the two zones once the initial flush had occurred. Elemental concentration patterns for eluents from the continuous flowing experiments were similar between columns from the two zones regardless of gas phase or temperature. In the episodically flushed columns, significant differences with respect to the eluent elemental concentrations were observed under the varying environmental conditions. These columns, which most closely resemble actual conditions on the basin, showed the dynamic nature of materials in response to alterations in saturation and oxidation state. In general, the column materials responded to the periodic wetting and drying cycles with great swings in elemental concentrations. The beginning of a cycle would generally correspond with high element concentrations in the eluents, followed by a decline through the wetting period, and a subsequent rebound to higher levels following a dry-down period. This is most likely a result of the deposition and resolubilization of reactive salts during drying and wetting cycles, respectively. The magnitude of this swing was influenced by both temperature and gas phase. The concentration gradient from beginning to end of a cycle was greatest at the higher temperatures for elements directly associated with pyrite oxidation (i.e. Fe and S), while species that may be influenced by subtle changes in redox (i.e. As and Se) responded more clearly to differences with respect to the gaseous composition.

These results suggest that the low pH fluids and high elemental concentrations emanating from materials in the 488-DAB are closely associated with environmental

factors that control dissolved and/or gaseous oxygen and to periodic wetting and drying events. As such, a dry cover should reduce the production of acid lechate over time if it is designed to retard or eliminate fluid flow and oxygen transport to the subsurface. In addition, the use of a cover to minimize the occurrence of evaporative salts on the landfills' surface may significantly reduce the contaminant load given that they are a major contributor of acidity in this system.

ACKNOWLEDGEMENTS

The authors would like to express their gratitude to Miles Denham with the Westinghouse Savannah River Technology Center for his assistance during this project. This work was funded in part by the U.S. Department of Energy (Financial Assistance Award DE-FC09-96SR18546) to the Savannah River Ecology Laboratory through the University of Georgia Research Foundation, Inc.

REFERENCES

1. Kleinmann, R.L.P. Acidic mine drainage: U.S. Bureau of Mines researches and develops control methods for both coal and metal mines, 1989, 161.
2. Nordstrom, D.K., Aqueous pyrite oxidation and the consequent formation of secondary iron minerals. *In*: J.A. Kittrick et al. (ed.) Acid sulfate weathering. SSSA Spec. Pub. No. 17, SSSA, Madison, WI, 1986, 223.
3. Singer, D.C., and W. Stumm, Acidic mine drainage: the rate determining step. Science, 119, 1121, 1970.
4. Stumm, W., and J.J. Morgan. Aquatic Chemistry, 2nd ed.,J. Wiley & Sons, New York, 1981.
5. Pierce, W.G., B. Belzile, M.E. Wiseman, and K. Winterhalder, 1994. Proceedings of the International Land Reclamation and Mine Drainage Conference, US Dept. of the Interior. SP06B-94, 148, 1994.
6. Evangelou, V.P, Pyrite Oxidation and its Control. CRC Press. Boca Raton, 1995.
7. Dobson, M.C., and A.J. Moffat, The Potential for Woodland Establishment on Landfill Sites. HSMO Press, 1993.
8. Lalvani, S.B., B.A. DeNeve, and A. Weston, Passivation of pyrite due to surface treatment. Fuel, 69, 1567, 1990.
9. Belzile, N., S. Maki, Y, Chen, and D. Goldsack, Inhibition of pyrite oxidation by surface treatment. Sci. of the Total Environ., 196, 177, 1997.
10. Allison, J.D., D.S. Brown, and K.J. Novo-Gradac, MINTEQA2/PRODEFA2, a Geochemical Assessment Model for Environmental Systems, Version 3.0 User's Manual, USEPA-Environmental Research Laboratory, Athens, GA, 1990.
11. Gee, G.W., and J.W. Bauder, Particle size analysis. *In*: A. Klute (ed.) Methods of Soil Analysis, Part 1: Physical and Mineralogical Methods, 2nd Edition. SSSA, Madison, WI, 1986, 393.
12. Bingham, J.M., and D.K. Nordstrom, Iron and aluminum hydroxysulfates from acid sulfate waters. *In*: C.N. Alpers et al (eds.) Reviews in Mineralogy and Geochemistry, Vol 40: Sulfate Minerals, Mineralogical Society *of* America, Washington, DC, 2000, 351.
13. Jambor, J.L., D.K. Nordstrom and C.N. Alpers, Metal-sulfate salts from sulfide mineral oxidation. *In*: C.N. Alpers et al (eds.) Reviews in Mineralogy and Geochemistry, Vol 40: Sulfate Minerals, Mineralogical Society of America, Washington, DC, 2000, 305.
14. Nordstrom, D.K., and H.M. May, Aqueous equilibrium data for mononuclear aluminum species. *In*: G. Sposito (ed.) The Environmental Chemistry of Aluminum, 2nd Edition, CRC Press/Lewis Publishers, 1996, 39.
15. Karathanasis, A.D., and W.G. Harris, Quantitative thermal analysis of soil materials. *In*: J.E. Amonette and J.W. Stucki (eds.) Quantitative Methods in Soil Mineralogy, SSSA, Madison, WI, 1994, 360.
16. Paulik, J.F., and M. Arnold, Simultaneous TG, DTG, DTA, and EG techniques for the determination of carbonate, sulfate, pyrite and organic material in minerals, soils and rocks. J. Thermal Anal., 25, 327, 1982.
17. Almeida, C.M.V.B., and B.F. Giannetti, Comparative study of electrochemical and thermal oxidation of pyrite. J. Solid State Electrochemistry, 6, 111, 2002.
18. Schwertmann, U., and R.M. Taylor, Iron oxides. *In*: J.B. Dixon and S.B. Weed (eds.) Minerals in the Soil Environment, 2nd Edition, SSSA, Madison, WI, 1989, 379.
19. Karathanasis, A.D., and B.F. Hajek, Revised methods for rapid quantitative determination of minerals in soil clays. Soil Sci. Soc. Am. J., 46, 419, 1982.
20. Tudor, D.N., Thermal Analysis of Minerals. Abacus Press, Kent, England, 1976.
21. Blowes, D.W., E.J. Reardon, J.L. Jambor, and J.A. Cherry, The formulation and potential importance of cemented layers in inactive sulfide mine tailings. Geochim. Cosmochim. Acta., 55, 965, 1991.
22. Nordstrom, D.K., C.N. Alpers, C.J. Ptacek., and D.W. Blowes, Negative pH and extremely acidic mine waters from Iron Mountain, California. Environ. Sci. Technol., 34, 254, 2000.
23. Garrels, R.M., and C.L. Christ, Solutions, Minerals, and Equilibria. Jones and Bartlette Publishers, Inc., Boston, MA, 1990.
24. Faure, G., Principles and Applications of Inorganic Chemistry. Macmillan Pub. Co., New York, NY, 1991.
25. Lindsay, W.L., Chemical Equilibria in Soils. John Wiley & Sons, New York, NY, 1979.
26. Elrashidi, M.A., D.C. Adriano, S.M. Workman, and W.L. Lindsay, Chemical equilibria of selenium in soils: A theoretical development. Soil Science, 144, 141, 1987.